Anomalous surface diffusion of protons on lipid membranes

Running Title: Anomalous proton surface diffusion

Maarten G. Wolf, Helmut Grubmüller and Gerrit Groenhof

Maarten G. Wolf
Theoretical and Computational Biophysics
Max-Planck-Institute for Biophysical Chemistry
Am Faßberg 11
D-37077 Göttingen, Germany

Helmut Grubmüller
Theoretical and Computational Biophysics
Max-Planck-Institute for Biophysical Chemistry
D-37077 Göttingen, Germany

Gerrit Groenhof
Computational Biomolecular Chemistry
Max-Planck-Institute for Biophysical Chemistry
Am Faßberg 11
D-37077 Göttingen, Germany

Current address:
Nanoscience Center & Department of Chemistry
University of Jyväskylä
P.O. Box 35
FI-40014 Jyväskylä
Finland
gerrit.x.groenhof@jyu.fi

Keywords: Excess proton, membrane, molecular dynamics, Hydyn, surface affinity, subdiffusion, superdiffusion

Anomalous surface diffusion of protons on lipid membranes

Maarten G. Wolf, Helmut Grubmüller and Gerrit Groenhof

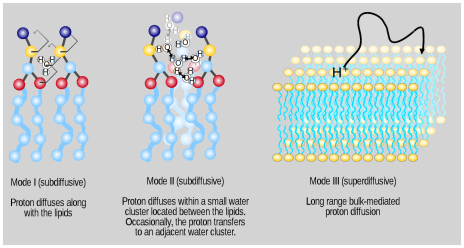

Abstract

The cellular energy machinery depends crucially on the presence and properties of protons at or in the vicinity of lipid membranes. To asses the energetics and mobility of a proton near a membrane, we simulated an excess proton near a solvated DMPC bilayer at 323 K, using a recently developed method to include the Grotthuss proton shuttling mechanism in classical molecular dynamics simulations. We obtained a proton surface affinity of 13.0 ± 0.5 kJ mol^{-1}. The proton interacted strongly with both lipid head group and linker carbonyl oxygens. Furthermore, the surface diffusion of the proton was anomalous, with a subdiffusive regime over the first few nanoseconds, followed by a superdiffusive regime. The time- and distance dependency of the proton surface diffusion coefficient within these regimes may also resolve many discrepancies between previously reported diffusion coefficients. Our simulations show that the proton anomalous surface diffusion originates from restricted diffusion in two different surface-bound states, interrupted by the occasional bulk-mediated long-range surface diffusion. Although only a DMPC membrane was considered in this work, we speculate that the restrictive character of the on-surface diffusion is highly sensitive to the specific membrane conditions, which can alter the relative contributions of the surface and bulk pathways to the overall diffusion process.

1 Introduction

The proton concentration gradient between two cellular compartments is an essential part of the cellular energy machinery. In combination with the transmembrane electrical potential difference ($\Delta\phi$), it generates a *protonmotive force* that is utilized to synthesize ATP [1]. Since measurements of the bulk-to-bulk *protonmotive force* correlate poorly with measured ATP yields [2, 3, 4], a simple chemiosmotic theory is inadequate. Hence, a steady state model has been proposed (ref [5, 4] and references therein), in which the cell continuously pumps protons across the membrane. These protons are then retained at the surface by a barrier that separates the surface volume from the bulk, so that a sufficiently high *protonmotive force* arises between the two faces of the membrane.

Recent equilibrium experiments [6, 7] and calculations [8, 9] have revealed that the proton concentration is indeed markedly higher on the membrane surface than in the bulk. In addition, a delay in surface-to-bulk as well as bulk-to-surface equilibration has been observed in kinetic experiments [10, 11, 12]. These data suggest the presence of a barrier, which separates the surface from the bulk, and thus support the steady-state model.

A wide range of diffusion coefficients have been reported for the proton on a lipid membrane. In experiments, in which protons were instantaneously released on the membrane, very fast diffusion of the proton over the surface has been measured ($3-12\cdot10^{-5}$ cm^2 s^{-1}) [11, 13, 14, 15], yet much lower surface diffusion has been observed in similar experiments ($0.034\cdot10^{-5}$ cm^2 s^{-1}) [10, 16] as well as NMR measurements ($0.44\cdot10^{-5}$ cm^2 s^{-1}) [17], equilibrium experiments ($0.02\cdot10^{-5}$ cm^2 s^{-1}) [6] and simulations ($0.15-0.23\cdot10^{-5}$ cm^2 s^{-1}) [8, 9]. The reported diffusion coefficients thus cover two orders of magnitude. To obtain more insight into the surface diffusion of the proton and to understand why such a wide range in diffusion coefficients has been observed, we have performed extensive simulations of a proton near a hydrated DMPC membrane.

In aqueous environments proton diffusion takes place via the Grotthuss mechanism, which in principle requires a quantum mechanical description. However, the timescales and system size required for simulating this process in a realistic model system preclude the use of quantum mechanical methods. Instead, we used the Hydyn simulation protocol [18], a method that includes explicit proton transfer in classical force field Molecular Dynamics simulations.

Although proton transfer to lipid head groups could be included in Hydyn as well, we have excluded this possibility in our simulations for two reasons: First, because efficient proton diffusion over the membrane surface seems to be independent of the availability of proton carriers in the form of buffer molecules [13] or lipid ionizable groups [14]. Second, because Yamashita and Voth, who used a protonatable Multi State Empirical Valence Bond (MS-EVB) model of dimethyl phosphate, have not observed any protonation of DOPC, DOPE, or DOPG lipids in their MD simulations of excess proton.[9] We obtained extensive sampling (app. 5 μs) by extended trajectories (50 ns), which yielded a converged proton density profile and allowed an in-depth investigation of the dynamic properties of an excess

proton near a DMPC lipid bilayer.

Our simulations revealed that the excess proton exhibits a completely downhill free-energy profile from bulk to surface. The proton surface density is approximately 200 times higher than in the bulk, which corresponds to a bulk-to-surface free energy difference of -13.0 ± 0.5 kJ mol^{-1}. This free-energy difference is in good agreement with previous results, from both experiments[6, 7, 10, 11] and computations[8, 9] and provides further support for the steady-state model, as well as for the notion of the membrane as a proton collecting antenna [6].

Furthermore, we found that proton diffusion over a lipid membrane surface is highly anomalous, with a subdiffusive regime over the first 1 ns, followed by a superdiffusive regime. The origin of the initial subdiffusive regime is the severely restricted diffusion of the proton on the surface by either strong binding to the lipids or entrapment inside small water clusters within the lipid head group region. The superdiffusive regime results from occasional excursions into the bulk solvent that lead to long-range surface diffusion. Due to the existence of a sub- and a superdiffusive regime, the proton surface diffusion coefficient is time- and length scale dependent, which could provide an explanation for the wide range of diffusion coefficients reported in the literature.

Regarding long-range surface diffusion, the low connectivity between the proton surface free-energy wells on a DMPC membrane impairs efficient on-surface diffusion. We speculate that the membrane conditions influence this connectivity and thus the diffusion via the on-surface pathway, providing a means to control the relative contributions of surface and bulk mediated diffusion to the overall diffusion process.This feature might even have influenced cell evolution with respect to the cellular energy machinery.

2 Methods

2.1 Proton transfer

To describe the excess proton we used the HYDYN protocol, a method that includes the Grotthus proton shuttling mechanism in MD simulations.[18] In HYDYN a proton acceptor is selected at regular intervals from among all possible acceptors around the current donor, using a Monte Carlo criterium that guarantees detailed balance. In between selection steps, the excess proton evolves on the free energy surface associated with proton transfer between the donor and the selected acceptor, using λ-dynamics.[19, 20] A proton transfer step is considered successful if at the end of this period, the proton resides on the acceptor. After this period, the evolution is terminated and a new acceptor is selected from among the molecules nearest to the molecule that now carries the excess proton. In this way, the excess proton can visit every protonatable site in the system, mimicking the Grotthuss mechanism. Because the selection and evolution steps maintain detailed balance, HYDYN simulations yield a correct thermodynamic ensemble.

The potential on which λ evolves is a linear interpolation between the potential energy functions of the reactant state (proton on donor) and product state (proton on acceptor). Therefore, during λ-dynamics, the system samples configurations in which the excess proton is either localized on a single water, forming a hydronium or Eigen complex, or delocalized over two waters, forming a Zundel complex. The relative populations of Eigen and Zundel states are in good agreement with *ab initio* simulations.[18] Although in bulk the excess proton is delocalized over several water molecules,[21], Voth and co-workers have shown that the two dominant EVB states involved in the interaction between an excess proton and a membrane surface correspond to the Eigen and Zundel complexes, [9, 8] which are both included in our simulations.

To keep the hydronium model compatible with the MM force field, the hydronium parameters are based on the water model used in our simulations (TIP3P[22]). These parameters were optimized to reproduce the main characteristics of an excess proton in small water clusters and in bulk water (supporting information).[23]

2.2 Simulation setup

We simulated 100 copies of a DMPC-membrane, modelled with the Berger force field[24] in TIP3P-water [22] including an excess proton for 50 ns each using Hydyn [18] (left graph in figure 1). In addition, we simulated 10 copies of the same membrane including a hydroxide (parameters were derived as described previously [23] and are available as supporting information) for 50 ns each with gromacs version 4.5.4 [25]. The system consisted of 64 lipids, 3658 water molecules and one hydronium or hydroxide in a 4.6 `x` 4.6 `x` 8.8 nm box. Here we focus on the hydronium and hydroxide only. Here we follow a strict bottom-up approach and focus on a single excess proton or hydroxide on a membrane surface without the additional complexity of ion-ion and ion-membrane interactions. Our approach to not include additional ions not only facilitates the interpretation but also avoid sampling problems, which are likely to occur due to competitive binding of the ions to the membrane. The excess proton or the hydroxide was initially positioned at the center of the water phase. In most excess proton simulations, the proton migrated to the membrane surface within 2 ns, after which occasional returns to the water phase were observed. Therefore, we used the last 48 ns of each trajectory for analysis.

The simulation setup was as follows. Bond distances were constrained using the SHAKE[26] and SETTLE[27] algortihm for hydronium/ lipids and water molecules, respectively. A time step of 2 fs was used. The Berendsen thermostat [28] with a τ_t of 0.5 ps was used to maintain a the temperature of 323 K, which is above the gel-to-liquid phase transition of DMPC (T_m = 296 K) and for which the lipid parameters have been validated.[24] The λ-particle, used to evaluate the proton transfer between two water molecules in Hydyn [18], was coupled to an Andersen heat bath [29] of 323 K with a coupling constant of 0.1 ps. The pressure was maintained constant at 1 atm using semi-isotropic coupling via the Berendsen barostat [28] with τ_p set to 2.5 ps and a compressibility of $4.5 \cdot 10^{-5}$

bar^{-1}. Van der Waals interactions were cut-off at 0.9 nm and the electrostatic interactions were treated using PME [30] with a real space cut-off of 0.9 nm and a reciprocal spacing of 0.12 nm. For the Hydyn simulations, neighbour searching was performed every step.

2.3 Analysis

To determine the number of lipid-hydronium hydrogen bonds, we considered all lipid oxygens as acceptors and the three hydronium hydrogens as donors. A hydrogen bond was considered present when the O_{lipid}-$O_{hydronium}$ distance was below 0.35 nm and the O_{lipid}-$O_{hydronium}$-$H_{hydronium}$ angle below 30 degrees.

The hydrogen bond existence function (either 0 when absent or 1 when present) was used to calculate the autocorrelation for each lipid-hydronium hydrogen bond. The hydrogen bond autocorrelation functions shown in this work are averages over all these individual autocorrelations.

The lateral mean square displacement (msd) of the hydronium was calculated for all trajectories except those that include a transition of the proton to the periodic image membrane. Furthermore, we removed the center of mass motion corresponding to the membrane leaflet the hydronium resided on. For the mean square displacement of the lipid atoms the values were calculated separately for the upper and lower leaflet, while removing the center of mass motion of the leaflet in question. Subsequently, the lipid mean square displacement of the lower and upper leaflet were combined.

For most observables, including msd, proton transfer rates, hydrogen bond autocorrelation function, we calculated the corresponding value x for each separate trajectory, and displayed the average $\overline{x} = \sum x/n$ and standard error $\sigma_{\overline{x}} = \sqrt{\sum (x-\overline{x})^2/n(n-1)}$. In cases where sampling was insufficient to determine a specific observable from one simulation, we combined 10 trajectories before calculating that observable. This was done for the hydronium free energy profiles and density plots.

3 Results

Proton diffusion in water can proceed either as an excess proton (H^+) via the Grothuss mechanims, or by reunion with a proton hole (OH^-) created by water auto-ionization. We modeled the excess proton and proton hole as a hydronium and a hydroxide, respectively. The density profile in figure 1 (right graph) and the free-energy profile in figure 2 show that the affinities for the membrane of these two species are very different. Hydronium has an increased affinity for the membrane surface, whereas the hydroxide has not and prefers the bulk. In this respect, the membrane surface is similar to the air/water interface, for which hydroniums also have affinity, but hydroxides not.[23] The surface affinity of the excess proton at the air/water interface, which had been predicted by Voth and co-workers on the basis of MS-EVB simulations,[31] has an enthalpic origin. We expect it to be stronger

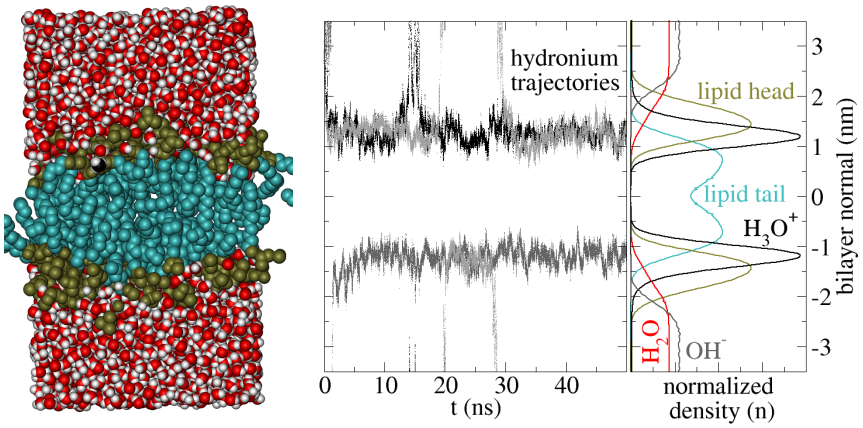

Figure 1: Excess proton near a membrane surface. Simulation box (left), examples of the time evolution of the excess proton along the bilayer normal (middle) and the ensemble average normalized number densities along the bilayer normal for the various components of the simulated system (right). The bilayer center is positioned at 0 nm and periodic boundary conditions connect the top and bottom of the graphs.

at the membrane surface than at the air/water interface because of specific hydrogen-bond interactions with the phospholipids, as we will show below. Because hydroxide does not bind to surface, we concentrated on the simulations of the excess proton rather than the proton hole.

The excess proton, after being released in the water phase of the DMPC-water system, moved to the membrane surface within two nanoseconds (for representative trajectories see middle graph of figure 1). In more than half of the simulations the proton remained at the surface for the rest of the 50 ns simulation time, whereas in the other simulations the proton made one or multiple brief excursions into the water phase before re-attaching onto the surface.

Such infrequent proton surface-desorption events require very long simulations to reach a converged ensemble. To check for convergence in our simulations, we compared the proton density profile on the lower and upper membrane leaflet and continued our simulations until the profiles matched. Sufficient convergence was reached after 4.8 μs.

As demonstrated by one of the representative trajectories in figure 1 (light grey middle graph), proton bulk excursions lead to occasional migration of the excess proton to the periodic image of the bilayer, which occurred in approximately 20 % of our trajectories. For ensemble properties these trajectories were simply added to the ensemble. For dynamic properties, however, we excluded these trajectories from our analysis, because the influence of the periodic image bilayer on the time-dependent observable would introduce systematic errors.

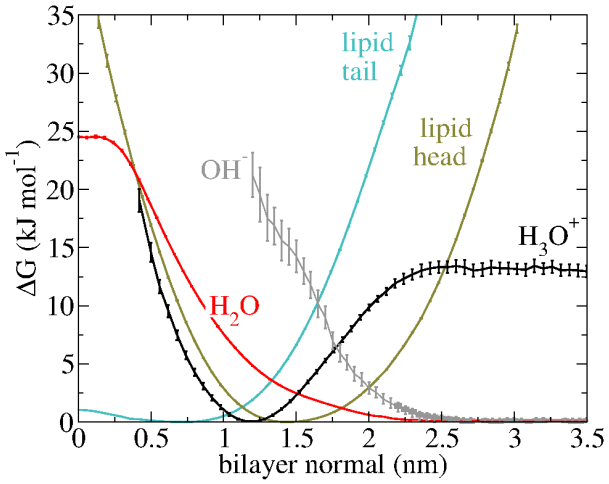

Figure 2: Free energy profiles along the bilayer normal demonstrate the strong proton surface affinity. The error bars denote the standard error.

3.1 Equilibrium distributions

The equilibrium distributions of the various components of the system, depicted in the right graph of figure 1, show that the hydronium has the largest normalized density at the interface, between the lipid head-group region and the lipid tail region. The water density at the hydronium's maximum density is already significantly reduced to 13 % of the bulk density. Nevertheless, despite the decreased number of excess proton carriers (*i.e.* water molecules) in the lipid-head group region (lower water density), the excess proton density in this region is found to be 200 times higher than in the bulk.

From these density profiles, we calculated free energy profiles via $\Delta G(z) = -RT \ln p(z)$ and a subsequent shift, with z the bilayer normal, R the gas constant, T the temperature (323 K), $p(z)$ the normalized number density at z. Figure 2 shows the resulting free energy profiles. The free energy difference for an excess proton moving from the water phase to the membrane surface is found to be -13.0 ± 0.5 kJ mol^{-1}, without a noticeable barrier in between. The free energy profile below 0.5 nm along the bilayer normal is not shown, because of insufficient sampling.

On the surface, the proton resides mostly in close proximity to the lipid's phosphate and carbonyl oxygens. The probability distribution of the minimum distance between the hydronium and the lipid oxygens ($d_{H-LipidO}$) clearly shows that the formation of such pairs is very favorable (first peak in figure 3). The hydronium interactions with both the phosphate oxygen of the lipid head group and the carbonyl oxygen of the lipid linker were equally populated, with an average interaction of one per hydronium for both (data not shown). The free-energy profile extracted from the probability distribution (inset in figure 3) revealed that a hydronium approaching a lipid oxygen already gains 5.8 ± 0.5 kJ mol^{-1}

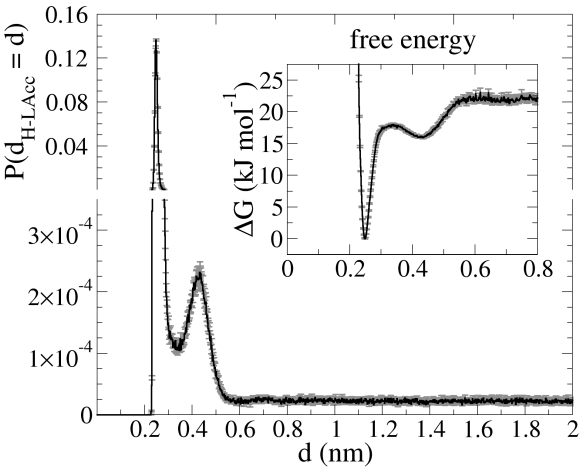

Figure 3: Probability distribution of the minimum distance between the hydronium and lipid oxygens. Inset is the associated free-energy profile. The very favorable interaction of a hydronium in direct contact with a lipid oxygen (low free energy at 0.25 nm separation) explains the strong proton surface affinity. The second peak shows that also a hydronium in a second solvation shell around a lipid oxygen is already favored over a bulk hydronium.

in the second solvation shell around a lipid oxygen. A small barrier of 2.0 ± 0.6 kJ mol^{-1} separates this first shallow minimum from the much deeper second free-energy minimum of 22 ± 0.5 kJ mol^{-1}, which arises from direct hydronium–lipid oxygen interactions. The observation that the proton can bind to the membrane surface in two distinct binding motives has also been observed in MS-EVB simulations by Voth and co-workers, who identified a shallow interface region, characterized by a hydronium interacting with two phosphate oxygens, and a deeper interface region, characterized by a Zundel complex interacting with the lipid carbonyls and phosphates. [9, 8].

3.2 Dynamics

The density profiles of figure 1 show that the excess proton is mostly located deeply within the head group region of the membrane. Like the water molecules within this region, the excess proton at the membrane surface is severely translationally restricted by the lipids, causing significantly slower diffusion over the surface than in bulk water. This was also observed in the MS-EVB simulations of an excess proton near lipid bilayers by Voth and co-workers.[9, 8] Furthermore, as the correlation between the mean square surface displacement and time deviates significantly from the linear relation characteristic for Fickian diffusion, as shown in in figure 4, the diffusion of the excess proton is highly anomalous. The power law exponent α of the relation $\left\langle \left[r\left(t\right) - r\left(0\right) \right]^2 \right\rangle \sim t^{\alpha}$ changes from 0.5 to 1.2

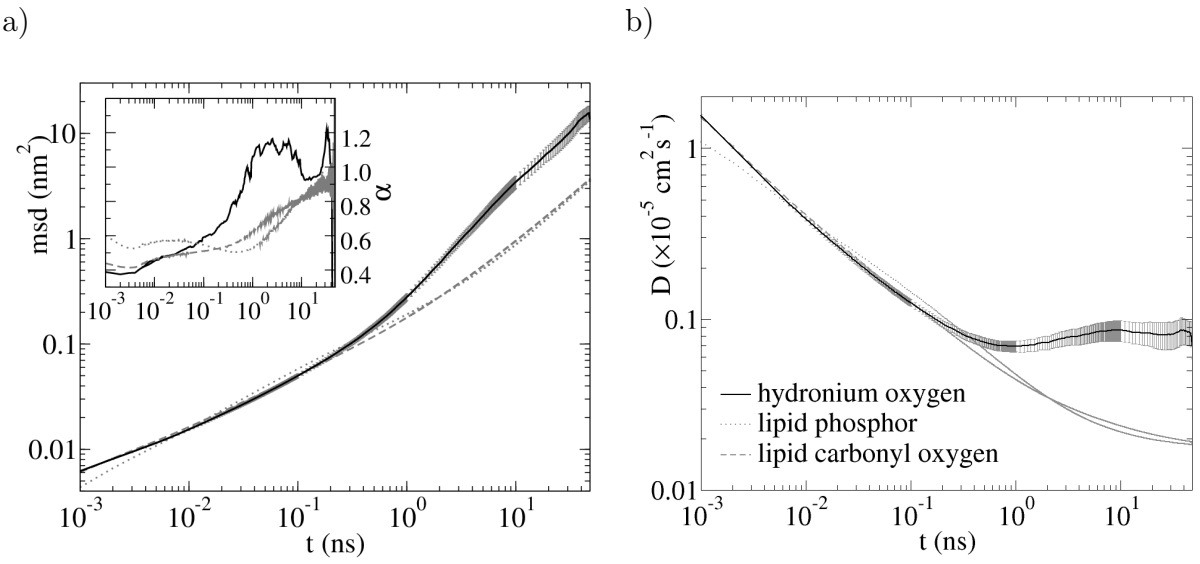

Figure 4: Surface diffusion of the hydronium oxygen (black), lipid phosphor (dotted grey) and lipid carbonyl oxygen (dashed grey). The error bars denote the standard error (which falls within the line width for the lipid atoms). (a) Mean square displacement. Inset is a 10-point running average of the power-law exponent α in $\left\langle [r(t) - r(0)]^2 \right\rangle \sim t^{\alpha}$ as a function of time t. (b) Time-dependent diffusion coefficient (equation 1). These graphs highlight the anomalous surface diffusion of a proton on a DMPC membrane.

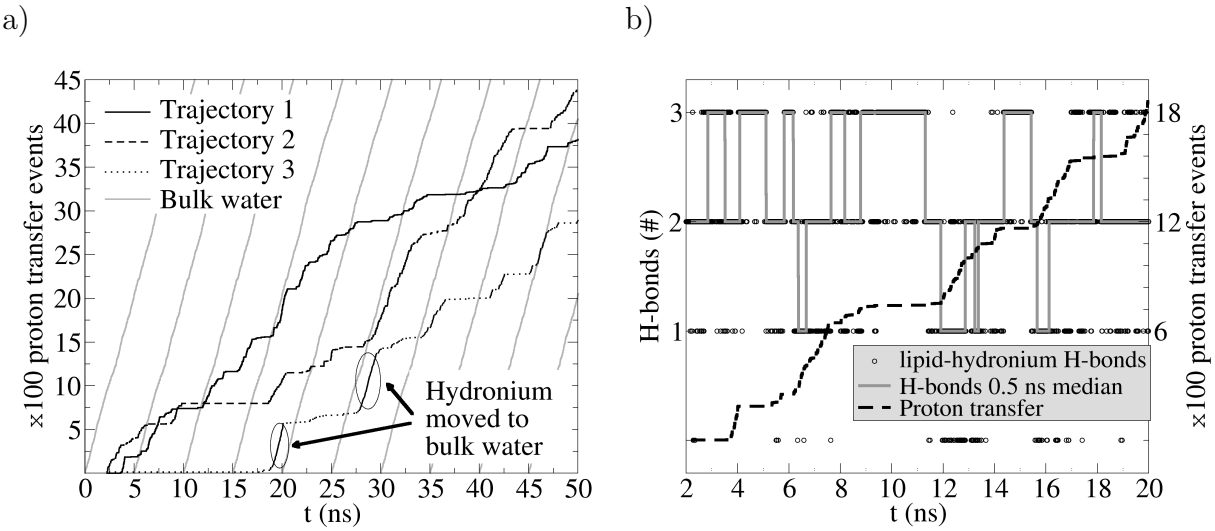

Figure 5: Proton transfer events at the membrane surface. (a) Comparison between the cumulative number of transfer events on the surface (three representative trajectories) and in the water phase (solid grey). For convenient comparison, the latter is shown multiple times, shifted 5 ns along the x-axis. (b) The correlation between proton transfer rate and lipid-hydronium hydrogen bonds. The correlation is most clear when the number of lipid-hydronium hydrogen bonds reaches its maximum, which is accompanied by almost absent proton transfer (plateau regions). Also the result of a 0.5 ns median of the lipid-hydronium hydrogen bonds, used for further analysis, is shown. For clarity, only 20 ns are displayed.

within the timeframe of our simulations (inset in figure 4 a). A plot of the self-part of the van Hove correlation function ($G_s(\mathbf{r}, t)$) in the supporting information shows that the probability distribution of the surface displacement is non-gaussian with a long tail, which also confirms that the diffusion is anomalous. A consequence of the anomalous proton surface diffusion is that the associated diffusion coefficient is not constant. Therefore, we calculated a time-dependent diffusion coefficient $D(t)$ instead via

$$D(t) = \frac{\left\langle [r\,(t) - r\,(0)]^2 \right\rangle}{2dt} \tag{1}$$

with d the number of diffusion dimensions. Figure 4 b shows that the time-dependent diffusion coefficient displays a minimum at 1 ns with a diffusion coefficient $D(1\text{ns})$ of $0.069 \pm 0.005 \cdot 10^{-5}$ cm^2 s^{-1}. After a short increase, the diffusion coefficient appears to level off after 10 ns at a diffusion coefficient $D(> 10\text{ns}) = 0.084 \pm 0.013 \cdot 10^{-5}$ cm^2 s^{-1}. For comparison, the proton diffusion coefficient in bulk water at 300 K is 4.4 cm^2 s^{-1} in Hydyn simulations [18].

		probability of x transfer ps^{-1}			
		none	1	2	3
number of	0	0.70	0.21	0.070	0.017
lipid-H_3O^+	1	0.85	0.094	0.044	0.010
hydrogen	2	0.95	0.028	0.017	0.003
bonds	3	1.00	0.001	0.000	0.000

Table i: Probability that a number x of proton transfer events take place within 1 ps.

In addition to the anomalous diffusion, our simulations revealed that the average proton transfer rate is significantly reduced from 0.42 ps^{-1} in the water phase [18] to 0.082 ± 0.024 ps^{-1} at the membrane surface. Furthermore, figure 5 a shows that in the presence of a membrane surface proton transfer occurs in bursts, whereas proton transfer in water is a continuous process. We identified two distinct phases for proton transfer on the surface: (1) a stall phase characterised by virtually no transfer events (plateau regions in figure 5 a), and (2) a transfer phase where the transfer rate approaches the one observed in the water phase.

Figure 5 b shows that the stall phase arises from a state, in which the hydronium forms three hydrogen bonds with lipids (for hydrogen bond definition see Methods section). Moreover, as the number of lipid-hydronium hydrogen bonds decreases, the probability of proton transfer increases (see table i). The average proton transfer rate in a state with 0, 1, 2 or 3 lipid-hydronium hydrogen bonds is 0.42, 0.23, 0.079 and 0.0012 ps^{-1}, respectively. We note that the transfer rate of a proton at the surface without lipid-hydronium hydrogen bonds is similar to that in bulk water. However, with a probability of 0.035, 0.12, 0.41 and 0.43 to be in a state with 0, 1, 2 or 3 lipid-hydronium hydrogen bonds, respectively, the contribution of states with relatively high transfer rates is small and the overall transfer rate is dominated by the states that exhibit slow transfer rates (states with 2 and 3 lipid-hydronium hydrogen bonds).

Since small fluctuations in the number of hydronium-lipid hydrogen bonds are always present, we used a 0.5 ns median (grey line in figure 5 b) to extract trajectories that correspond to 0, 1, 2 or 3 hydronium-lipid hydrogen bonds, respectively, for further analysis of the proton surface diffusion. Figure 5 b shows that the length of the stall phase agrees very well to a continuous stretch of median 3 hydrogen bonds, suggesting that the 0.5 ns median is an appropriate measure. Also the proton transfer rate, with 0.38, 0.22, 0.097 and 0.0058 ps^{-1}, and the occupancy, with 0.02, 0.10, 0.46 and 0.41, extracted from the trajectory parts with a median value of 0, 1, 2 or 3 lipid-hydronium hydrogen bonds are close to the values obtained in a direct analysis (previous paragraph). From now on, we will refer to the ensembles of trajectory parts that correspond to 0, 1, 2 or 3 (x) median hydronium-lipid hydrogen bonds as hb0, hb1, hb2 or hb3 (hb$x$).

The representative trajectory illustrating the proton transfer stall phase (figure 5) already shows that the lifetime of a specific number of hydrogen bonds can be in the order

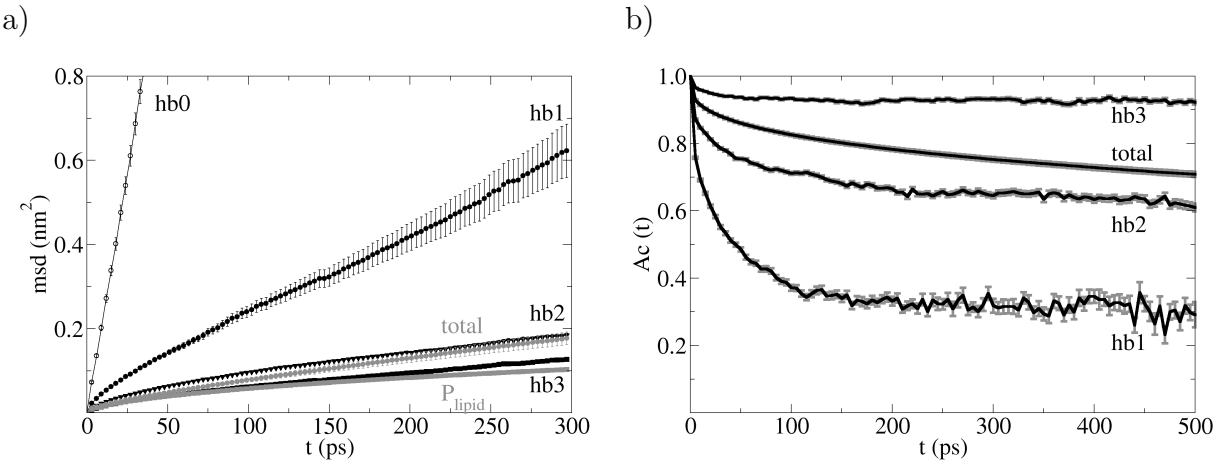

Figure 6: Restricted diffusion of an excess proton hydrogen-bonded to a lipid. Properties of the hb**x** ensembles, demonstrating the importance of the number of hydrogen bonds for the dynamics of the proton. (a) Lateral mean square displacement. For comparison, also the total hydronium and the lipid phosphor msd is displayed. (b) Autocorrelation function of the hydronium-lipid hydrogen bonds, which remarkably decays to a plateau.

of nanoseconds. Analysis of the lifetime distribution revealed a half life for the existence of 0, 1, 2 and 3 lipid-hydronium hydrogen bonds of 0.63, 0.37, 0.69 and 0.87 ns, respectively. In addition, 2 and especially 3 lipid-hydronium hydrogen bonds exhibited a very long tail in the lifetime distribution, with more than 10 percent having a lifetime that exceeded 4 ns.

Further analysis of the hb**x** ensembles revealed that the msd of hb3 was, within statistical error, equal to the lipid phosphor (figure 6 a), reaching a msd after 300 ps of 0.13 ± 0.05 nm^2 and 0.10 ± 0.01 nm^2, respectively. A larger difference was found for hb2 and hb1, with 0.18 ± 0.01 and 0.62 ± 0.06 nm^2, respectively. Without hydronium-lipid hydrogen bonds, the msd is larger still with 7.8 ± 0.6 nm^2. Thus, only hydroniums that have three hydrogen bonds to lipids follow the lipid diffusion.

Although the hydronium remains bound to a median of 1 or 2 lipids in the hb1 or hb2 ensemble, respectively, the autocorrelation of the hydronium lipid contact (see Method section for details), shown in figure 6 b, indicates that the hydronium moves between different lipids. In the hb3 ensemble, more than 90% of the hydronium-lipid hydrogen bonds still exist after 500 ps. In contrast, for the hb1, and to a lesser extent the hb2 ensemble, the autocorrelation function drops significantly for the first 100-200 ps, indicating hydrogen bond interactions with different lipids.

Remarkably, the decay in the autocorrelation reaches a plateau after $\sim$250 ps (figure 6 b). For the timespan shown in figure 6 b, we can exclude a finite size effect as a

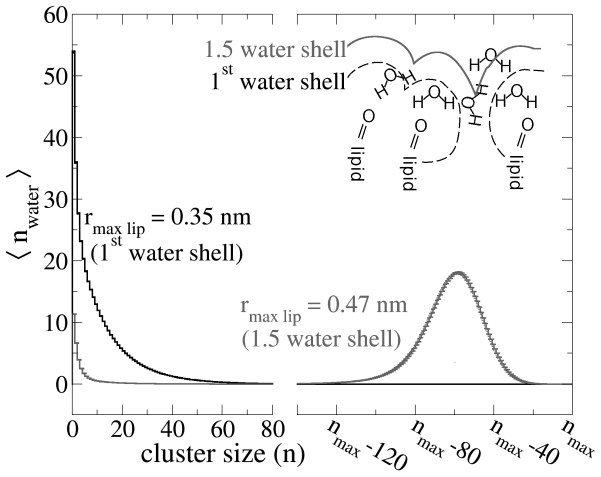

Figure 7: Connectivity of the water molecules at various distances around lipid oxygens. Cluster size distribution for water molecules within 0.35 nm and 0.47 nm from a lipid hydrogen bond acceptor, corresponding to first solvation shell and 1.5 water solvation shell, respectively. n_{max} is the total number of water molecules within the considered water shell. (Inset) Schematic representation of the water shells considered in the cluster analysis.

cause [32, 33], because the probability that the hydronium-lipid hydrogen bond is restored by an interaction with a periodic image is negligible (see supporting information). The hydronium-lipid interaction thus switches between a few lipids.

As the proton is mainly located on water molecules in direct contact with lipid oxygens, the connectivity of these water molecules likely plays a crucial role in the hydronium-lipid hydrogen bond autocorrelation function. To assess this connectivity, we extracted the cluster-size distribution of all the water molecules within the first solvation shell and 1.5 water solvation shell, respectively, (for schematic representation see inset in figure 7). Water molecules were considered part of a cluster if the distance to any member of the cluster is within 0.35 nm. Figure 7 shows that, when considering only the first solvation shell around lipid oxygens, many small clusters were present, demonstrating a low connectivity of these water molecules. In contrast, as soon as at least one additional water layer was considered (1.5 water solvation shell), the dominant cluster size was close to the maximum cluster size, suggesting one large water network. Since proton transfer to a second shell water molecule already results in a severe free-energy penalty (figure 3), the small clusters of first-shell water molecules create small free-energy wells in which the proton freely diffuses, but only rarely escapes. As a result, the proton repeatedly revisits the lipids around the free-energy well.

Despite the free-energy barrier between these small water clusters, we observed occa-

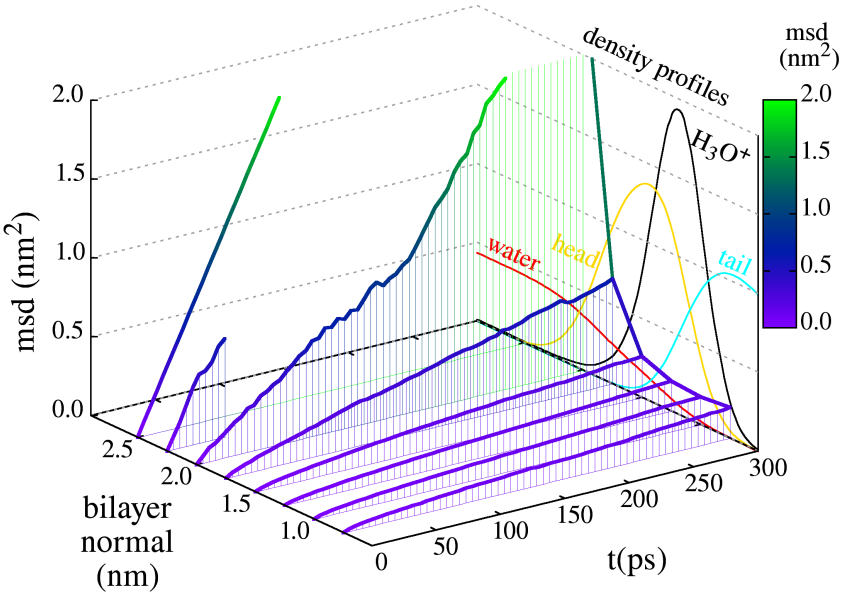

Figure 8: Lateral mean square displacement of the excess proton at various membrane penetration depths shows that the diffusion rate increases as the proton leaves the membrane. The msd at 2.5 nm is the average lateral msd in bulk water and we could only obtain the msd at 2.25 nm over 50 ps due to sampling problems. To illustrate the excess protons penetration depth the density profiles normal to the membrane surface of the hydronium, water, lipid tails and lipid head groups are plotted in the background (also shown in figure 1).

sional transitions of the proton between adjacent free-energy wells (see figure 9 for representative trajectory), presenting an on-surface diffusion pathway. The low transition rate and relatively long dwell time inside the free-energy wells closely resembles diffusion near the percolation threshold, which yields subdiffusive behavior [34].

Finally, the proton occasionally leaves the bilayer center, diffuses along the outermost boundary of the surface or even through the water phase, before re-adsorbing onto the bilayer. Figure 8 shows that the dynamics of a proton in this non-surface-bound state approaches that of a proton in bulk, both with respect to diffusion coefficient and transfer rate.

Thus, from our simulations we have identified three modes in which the proton diffuses: (i) bound directly to a lipid, (ii) shuttling inside the small water clusters within the head group region with occasional hops to nearby clusters, and (iii) through the bulk. The two lipid-bound diffusion pathways have also been identified in MS-EVB simulations.[9, 8] To illustrate the effect of the different diffusion modes we have described for proton

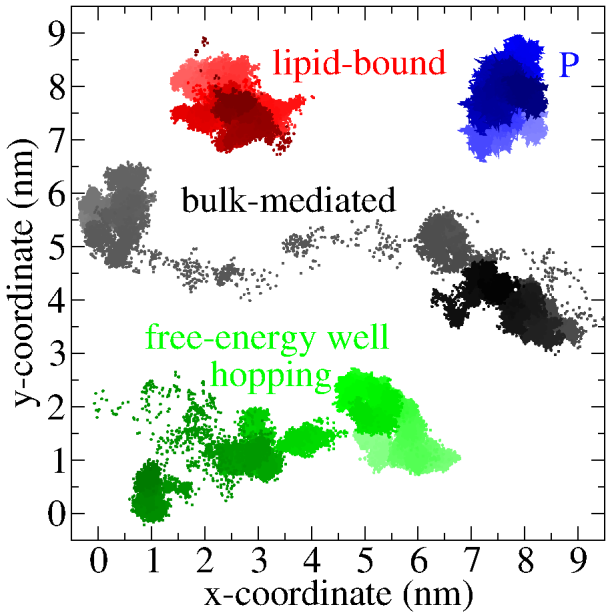

Figure 9: Representative trajectories of the displacement of the excess proton when it is bound to a lipid, hopping between free-energy wells and in bulk. For comparison also a typical lipid phosphor trajectory is shown. The time intervals are from 2 ns (light) to 50 ns (dark).

displacement, representative trajectories are displayed in figure 9. A lipid-bound proton exhibited the same restricted diffusive behavior as the lipid phosphor and, as a result, the diffusion coefficient at short timescale is very low. In contrast, both a proton that hopped between adjacent free-energy wells and a proton that moved through the bulk covered considerably larger distances. Although proton desorption from the lipid membrane as well as hopping between free-energy wells are rather infrequent, the much larger diffusion coefficient associated with these diffusion modes causes an increase of the overall diffusion coefficient at larger timescale (a superdiffusive regime).

The msd in figure 4 indeed shows a superdiffusive regime, but only for a very short timespan. For bulk-mediated surface diffusion, however, the diffusion coefficient is expected to increase asymptotically towards the bulk diffusion coefficient, due to the growing contribution of the bulk-mediated diffusion pathway in time. In our simulations, the small solvent volume restricts this growing contribution, as the protons that reach the periodic image membrane are effectively removed from the bulk. To address the contribution of the reduced solvent volume, we numerically solved the 2D diffusion equation for a proton released on a membrane surface that consisted of periodic low-free-energy wells, schematically shown in figure 10. Parameters in this model were derived from our atomistic simulations (for details see supplementary information). Figure 10 shows that the mean square surface displacement of a proton in this simplified system displays an initial subdiffusive regime, in agreement with our atomistic simulations. As expected for bulk-mediated diffusion, at long timescales an extended superdiffusive regime that approaches bulk diffusion asymptotically appears. When we reduced the volume in our simplified model by introducing a second membrane (figure 10), the timespan of the superdiffusive regime is significantly reduced, in agreement with the atomistic simulations. The short superdiffusive regime in our atomistic simulations is thus a result of the small periodic system, and not a typical property of proton diffusion on a membrane surface.

4 Discussion & Conclusion

We have performed extensive molecular dynamics Hydyn simulations[18] of a single excess proton in the presence of a DMPC bilayer and analysed proton free energy profiles normal to the membrane as well as the proton surface diffusion, which are key aspects of the steady-state theory put forward to explain the observed *protonmotive forces* in the cellular energy machinery (ref [5, 4] and references therein).

4.1 Equilibrium distributions

In our Hydyn simulations full convergence was achieved with respect to the proton density distribution normal to the membrane. The free-energy difference for a proton moving from the bulk to the membrane surface was found to be -13.0 ± 0.5 kJ mol^{-1}. Previous

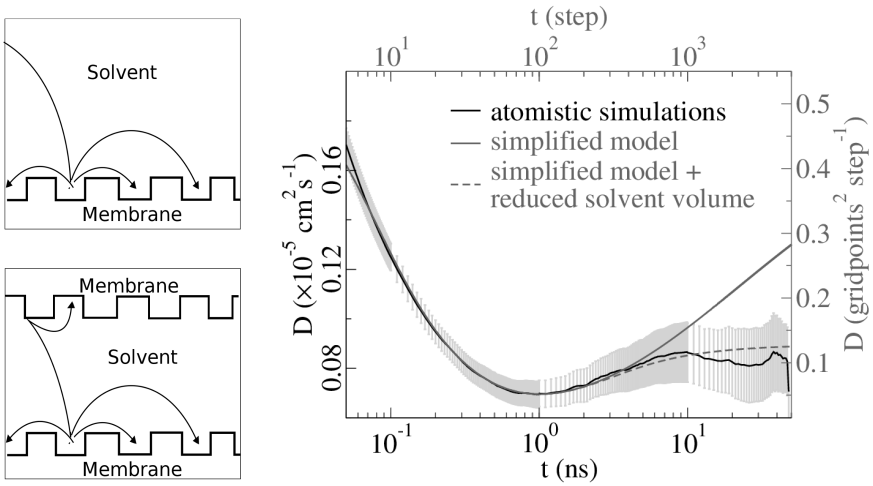

Figure 10: Schematic representation of our simplified model with infinite solvent volume (upper left) and a reduced solvent volume (lower left). In the right graph, the time dependence of the surface-diffusion coefficient as derived by the simplified model (grey) shows the expected increasing diffusion coefficient at long timescale for infinite solvent volume (solid) and the effect of a reduced volume (dashed). The latter is in agreement with the result of our atomistic simulations (black). The lower and left axis correspond to the atomistic simulations and the upper and right axis correspond to the simplified model. For simplified model details see supplementary information.

simulation studies have reported proton free-energy differences between surface and bulk of -21, -3 and 42 kJ mol^{-1} at a DOPC, DMPC and DLPE bilayer, respectively [9, 8, 35]. However, these simulations were performed at a different temperature (300 K) than ours (323 K). Therefore, a direct comparison, even in the case of DMPC is difficult. Moreover, also different force fields and different approaches to model the excess protons were used. With these differences in mind, we consider our results in reasonable agreement with the MS-EVB simulations from Voth and co-workers[8]. Nevertheless, the results of our simulations demonstrate that very long trajectories are required to get converged results and a classical protocol for proton transfer is an advantage in this respect.

A comparison with experiments is even more complicated, because direct measurement of the proton surface concentration [H^+] is a formidable challenge. Recently, the local proton exchange dynamics at DOPC and DOPG lipid vesicle surfaces in thermodynamic equilibrium has been measured. Although the membrane is different in these experiments, it was found that the proton surface concentration is 100-fold larger than the bulk concentration, corresponding to a proton surface affinity of -11.5 kJ mol^{-1} [6, 7], in line with our result.

In our simulations, the excess proton on the membrane surface interacts strongly with the lipid's oxygens in the head group phosphate and linker carbonyl. Strong interactions have also been observed between the lipid oxygens and adjacent water molecules [36, 37, 38, 39, 40]. If we assume that an excess proton associated with such a water molecule experiences a similar strong lipid interaction, association of the excess proton with a water molecule adjacent to a lipid oxygen will be preferred over a bulk water molecule, which could (partly) explain the strong proton surface affinity. We speculate that this preference of the proton for a water molecule interacting with the lipid oxygen over a bulk water molecule is a general feature of lipid membranes, because (1) a strong proton surface affinity has been found for other lipid bilayers, both in measurements [14, 7, 6] and simulations [9, 8] and (2) water molecules that interact strongly with lipids have been observed in other lipid membranes.[36]

Since the proton interacts equally strong with the phospate oxygens of the head group and the carbonyl oxygens of the linker, not only the lipid head group should be considered in the discussion about the proton surface properties, but also the lipid linker group. In fact, the observation that proton surface properties are relatively insensitive to the lipid headgroups [14] may be attributed to a strong proton-lipid linker interaction. It would be interesting therefore to repeat these experiments with a distinct lipid linker that has no or limited capability to stabilize the proton within the lipid bilayer.

4.2 Dynamics

Movement of the proton on the membrane surface is not the 2D equivalent of proton diffusion in bulk water. Instead, the diffusion in presence of a membrane surface is highly anomalous, characterized by a short subdiffusive regime (1 ns) and a subsequent superdif-

fusive regime. The anomalous diffusion is due to presence of three different diffusion processes (figure 11), each with a distinct diffusion coeffient.

In the first diffusion process, the hydronium is tightly bound to the lipid and follows the diffusion of the lipid, which is subdiffusive at short timescales.[41] In the second process, protons are less tightly bound inside small water clusters within the lipid headgroup region and occasionally jump from one cluster to another. Although the distance between the clusters is small (approximately one water molecule, in agreement with experiment[17]), the transition frequency is rather low due to a significant barrier separating the clusters. Within these clusters, the proton shuttles between the water molecules, experiencing a local caging effect. This caging effect in combination with occasional jumps between clusters generates a percolation effect, which leads to a subdiffusive regime on short timescales and normal diffusion at long timescales.[34, 41] These two diffusion modes, in which the proton's movement is correlated with the movement of the lipids have also been identified by Voth and co-workers, who attributed the overall diffusion of an excess proton to a slow diffusion of protons trapped within the headgroup region and a slightly faster diffusion of protons in the shallow interface region before bulk water.[9, 8].

Finally, in the third process, the proton resides on the outer edge of the headgroup region and escapes into the bulk, where the diffusion constant approaches that of a free excess proton in water. For bulk-surface systems that exhibit strong surface adsorption, the adsorption-desorption kinetics frequently provides the primary mechanism of surface diffusion, which, in case of a surface diffusion that is slower than bulk diffusion, gives rise to a superdiffusive regime [42]. The superdiffusive regime therefore exists due to the strong surface adsorption of the proton in combination with the severely restricted diffusion in the surface-bound states.

An important consequence of the sub- and superdiffusive regime is that the diffusion coefficient is not constant. Yet, previous reports on diffusion coefficients of protons at membranes surfaces have assumed a constant value corresponding to Fickian diffusion [8, 9, 11, 13, 14, 17, 10]. Interestingly, the measured diffusion coefficients ($0.02 - 12 \cdot 10^{-5}$ cm^2 s^{-1}) cover a similar range as the time-dependent diffusion coefficient in our simulations ($0.069 - 9 \cdot 10^{-5}$ cm^2 s^{-1}). However, leaving out the proteinaceous systems from the comparison worsens the agreement, as the diffusion constants reported for pure phosphatidyl-choline systems are typically much higher.[13, 14]

To compare our results to previous computations, we extracted a constant diffusion coefficient from a 1-10 ps time interval as in ref [8, 9], and obtained a value of $0.32 \cdot 10^{-5}$ cm^2 s^{-1}. Because we performed the simulation at 323 K, rather than at 300 or 298 K, at which most experiments and MS-EVB simulations were carried out, we cannot directly compare the diffusion constants. Since tunneling does not play a dominant role near room temperature, we can assume Arrhenius behaviour and expect the diffusion to be lower at room temperature. However, because our results were obtained under periodic boundary conditions, the diffusion is underestimated due to finite size artifacts,[43] which are not easily corrected in a non-homogeneous system, such as ours. Although the correction may

affect the diffusion through bulk and on the membrane surface differently because of the larger hydrodynamic radius of the phospholipids compared to water, we consider it highly unlikely that the anomalous character of the diffusion would disappear after correction. Nevertheless, even with these issues in mind, the diffusion constant is in line with the MS-EVB result of $0.15 - 0.23 \cdot 10^{-5}$ cm^2 s^{-1} [8, 9]. We remark at this point that despite the apparent agreement with previous MS-EVB results, our approach underestimates proton delocalization, which affects solution structure (Fig 18, Supporting Information) and may also have an impact on the diffusion process. At present, the MS-EVB3 approach by Voth and co-workers is presumably the most suitable approach to take into account the effect of charge delocalization in classical MD simulations of protons.[21] Thus, to confirm the anomalous proton diffusion, one would need to perform sufficiently long MS-EVB simulations in the future.

Experimental support for the existence of bulk-mediated long-range proton surface diffusion is ambiguous. On the one hand, fast proton surface diffusion in systems with low aqueous buffer concentration is incompatible with predominant bulk-mediated long-range surface diffusion via the buffer molecules[14, 15]. In addition, a H/D kinetic isotope effect of five shows that hydrogen bond breaking is rate limiting rather than water rearrangement, suggesting on-surface diffusion via water-wires as the dominant diffusion mode [14, 15]. Furthermore, faster proton on-surface than surface-to-bulk displacement [6] and the slow detection of protons appearing in the bulk after release on a purple membrane surface, as opposed to the fast detection of the proton appearing at a new surface site [10, 11, 12], indicates fast on-surface diffusion and no significant contribution of bulk-mediated diffusion to the surface diffusion. On the other hand, a theoretical assessment shows that protons desorb and re-adsorb onto the surface thousands of time before equilibration into the bulk, giving rise to coupled surface bulk diffusion [44]. If the rate-limiting step for desorption is breaking of a hydrogen bond to escape the free-energy well, the many desorbtion events will induce a H/D kinetic isotope effect between 2.5 and 7, providing an alternative explanation for the observed isotope effect. In addition, in fluorescence measurements at high aqueous buffer concentrations the diffusion rate is compatible with bulk-mediated proton diffusion via the buffer molecules [14, 13]. Furthermore, lateral on-surface proton diffusion on DPPC bilayers could not be detected by scanning electrochemical microscopy proton feedback [45].

We suspect the existing conundrum on the existence of the bulk-mediated diffusion pathway originates from the fact that the competing on-surface pathway is very sensitive to the membrane conditions. On the one hand, in our simulations, the low connectivity of the first shell water molecules severely limits long-range on-surface diffusion of the proton, promoting the bulk-mediated diffusion pathway. On the other hand, the protein content in a purple membrane, for example, may promote the on-surface diffusion mode over bulk-mediated long-range surface diffusion, as observed in experiments [10, 11, 12]. On langmuir films, a similar promotion may be achieved by compression [46].

In fact, we expect that the overall proton surface diffusion is sensitive to factors that influence any of the observed diffusion modes, either in diffusion behavior or relative pop-

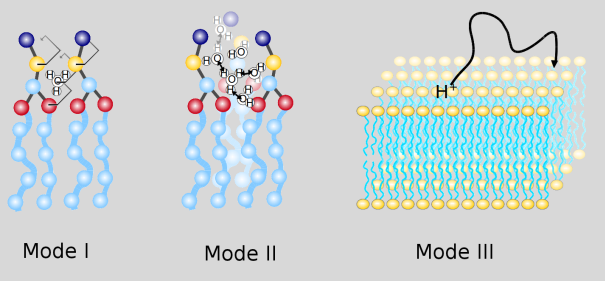

Figure 11: Schematic representation of the three observed diffusion modes for a proton on a membrane surface. In Mode I the hydronium is bound to the lipids. Proton transfer is absent and diffusion is determined by the lipid, to which it is bound. In Mode II the proton is captured within a free-energy well composed of a small lipid-enclosed cluster of water molecules. Within this well the proton can transfer freely, and diffusion is a superposition of the proton diffusion within the well, and the diffusion of the whole well. In Mode III the proton desorbes from the membrane. The proton migrates freely over the surface or through the bulk before the proton readsorbes onto the membrane, leading to largescale surface diffusion.

ulation. For example, conditions that influence the well-depth associated with the isolated water clusters, for instance by competition of other ions, might have a significant impact on the proton surface dwell time. In this respect, we note that the cations present in the buffer solution may be relevant, as sodium is attracted to the lipid bilayer surface, occupying the same water clusters as the proton [47, 48, 49, 50, 51, 52, 53, 54, 55, 56, 57], whereas potassium has no significant affinity for the membrane surface or at least less than sodium [52, 49, 56, 54]. These observations suggest that the membrane composition as well as the constituents of the solution medium could also strongly affect proton surface diffusion.

To validate proton anomalous surface diffusion experimentally, the relation between time and msd is required, particularly within the time- and lengthscale, in which the sub- and superdiffusive regime are clearly identifiable. Therefore, the experimental time- and lengthscale should be within a few tens of ns and nm^2, which corresponds to a distance between a proton source and a proton sensor of at maximum a few tens of lipids.

To control the distance between a proton source and a proton sensor on the nm length scale one can think of a rigid linker. Clearly, the resulting linked source and sensor cannot be allowed to interact with other linked pairs, which requires very low concentrations and careful design of the linker to avoid aggregation, presenting a considerable challenge. Yet, with a proper linker the existence of a superdiffusive regime can be tested by varying the length of the linker within the relevant length scale. If the linker distance falls within the superdiffusive regime, a super-linear relation between the square of the linker distance and the time of maximum sensor activity should be observed.

Alternatively, in an ensemble of single molecule experiments, in which a single proton

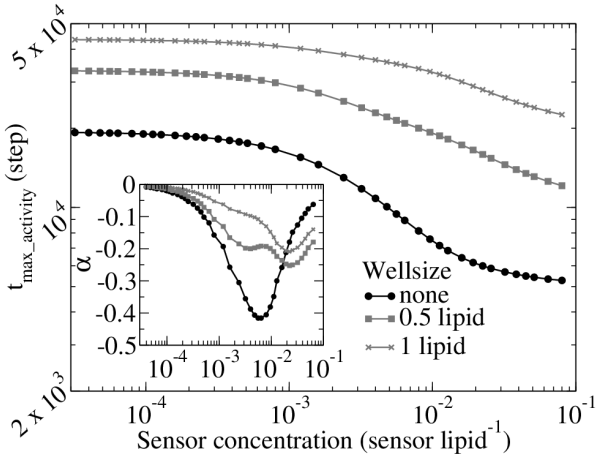

Figure 12: Time to maximum sensor activity after proton release on the surface as a function of the sensor concentration. The loglog scale revealed a power law relation in the well systems (grey), which is absent for free surface diffusion (black). The plot of the power law exponent α shows that the power law relation is only approximate.

is released on a membrane, the ensemble-averaged travel distance to a sensor depends on the sensor concentration. Normal and anomalous diffusion will then induce a different response of the time to maximum sensor activity to variation of the concentration, which may for instance be probed by super-resolution imaging techniques [58, 59]. As an example, we calculated this response in our simplified model with the proton source distributed on an evenly spaced grid (for details see supplementary info). Figure 12 shows that the predominant on-surface diffusion can be clearly distinguished from the predominant bulk-mediated diffusion in this way.

4.3 Implications for the cellular energy machinery

With respect to the cellular energy machinery, a steady-state theory has been put forward to explain the measured *protonmotive forces*, which requires a barrier that prevents fast proton transfer from the membrane surface to the bulk water phase. The lower free energy of a proton on a membrane-surface with respect to a proton in water that we have extracted from our calculations fulfills this criterium.

We observed a minimum proton surface diffusion coeffient at 1 ns of $0.069 \pm 0.005 \cdot 10^{-5}$ cm^2 s^{-1}, which is sufficient for the energy machinery to function, as illustrated by the following example. With a conservative estimate of the average ATPase density of $1.5 \cdot 10^{12}$ cm^{-2} [60, 61], it will take the proton on average 480 ns to reach an ATPase at minimum diffusion speed. However, the time-dependent diffusion coefficient at 480 ns is much larger than the observed minimum, so the actual travel time from pump to ATPase is much

shorter. In addition, on a functional cell membrane many other effects will reduce this travel time significantly, such as the proton pump density, clustering of relevant proteins [62], formation of cristae and the antenna effect of the protein [63].

Nevertheless, bulk-mediated proton surface diffusion inevidently results in proton loss into the bulk, which, particularly in cells without mitochondria, reduces the efficiency of the cellular energy machinery. These cells will therefore greatly benefit from an effective proton antenna effect, which requires one extended volume that attracts and shuttles protons over a significant distance, similar to the coulomb cage appearing at titratable amino acids that act as antennae in proteins [64, 63]. However, in our simulations, the small water clusters in which the proton resided were mainly unconnected and proton transitions between clusters were rare. As a result, long-scale diffusion via these free-energy wells is slow.

The connectivity of these water clusters is mostly lost due to the relatively bulky PC head groups. We speculate that the presence of smaller head group lipids in the membrane will increase the connectivity, thereby creating funnels for proton diffusion on the membrane surface and promoting the on-surface diffusion mode. Examples of such lipids are phosphatidylethanolamines (PE) and cardiolipin (CL). Experimentally, proton diffusion on a PE membrane is approximately two times faster than on a PC membrane [13, 14, 15]. Furthermore, both PE and CL have been found abundantly in membranes involved in the cellular energy machinery [65, 66, 67]. Thus, in addition to the observed structural benefits for the proteins involved in the respiratory chain [67, 65] as well as the proton buffer capacity [66], PE and CL may increase the range of the proton on-surface diffusion, which will result in a more efficient energy machinery and allow the cell to withstand harsher conditions.

Acknowledgement

We thank Peter Pohl for valuable discussions. This work was funded by the Volkswagen Foundation, grant 83940. MGW was supported by the Humboldt Foundation and GG is supported by the Academy of Finland.

Supporting citations

Reference [68] appears in the Supporting Material.

References

[1] Roderick A. Capaldi and Robert Aggeler. Mechanism of the F_1F_0-type ATP synthase, a biological rotary motor. *Trends Biochem. Sci.*, 27:154–160, 2002.

[2] T.A. Krulwich, M. Ito, R. Gilmour, M.G. Sturr, A.A. Guffanti, and D.B. Hicks. Energetic problems of extremely alkaliphilic aerobes. *Biochim. Biophys. Acta*, 1275:21–26, 1996.

[3] H. Michel and D. Oesterhelt. Electrochemical proton gradient across the cell membrane of *Halobacterium halobium*: comparison of the light-induced increase with the increase of intracellular adenosine triphosphate under steady-state illumination. *Biochemistry*, 19:4615–4619, 1980.

[4] Armen Y. Mulkidjanian, Joachim Heberle, and Dmitry A. Cherepanov. Protons @ interfaces: Implications for biological energy conversion. *Biochim. Biophys. Acta - Bioenergetics*, 1757:913–930, 2006.

[5] Dmitry A. Cherepanov, Boris A. Feniouk, Wolfgang Junge, and Armen Y. Mulkidjanian. Low dielectric permittivity of water at the membrane interface: Effect on the energy coupling mechanism in biological membranes. *Biophys. J.*, 85:1307–1316, 2003.

[6] M. Brändén, T. Sandén, P. Brzezinski, and J. Widengren. Localized proton microcircuits at the biological membrane-water interface. *Proc. Natl. Acad. Sci. USA*, 103:19766–19770, 2006.

[7] T. Sandén, L. Salomonsson, P. Brzezinski, and J. Widengren. Surface-coupled proton exchange of a membrane-bound proton acceptor. *Proc. Natl. Acad. Sci. USA*, 107:4129–4134, 2010.

[8] A.M. Smondyrev and G.A. Voth. Molecular dynamics simulation of proton transport near the surface of a phospholipid membrane. *Biophys. J.*, 82:1460–1468, 2002.

[9] T. Yamashita and G.A. Voth. Properties of hydrated excess protons near phospholipid bilayers. *J. Phys. Chem. B*, 114:592–603, 2010.

[10] J. Heberle, J. Riesle, G. Thiedemann, D. Oesterhelt, and N.A. Dencher. Proton migration along the membrane surface and retarded surface to bulk transfer. *Nature*, 370:379–382, 1994.

[11] U. Alexiev, R. Mollaaghababa, P. Scherrer, H.G. Khorana, and M.P. Heyn. Rapid long-range proton diffusion along the surface of the purple membrane and delayed proton transfer into the bulk. *Proc. Natl. Acad. Sci. USA*, 92:372–376, 1995.

[12] Oksana A. Gopta, Dmitry A. Cherepanov, Wolfgang Junge, and Armen Y. Mulkidjanian. Proton transfer from the bulk to the bound ubiquinone Q_B of the reaction center in chromatophores of *Rhodobacter sphaeroides*: Retarded conveyance by neutral water. *Proc. Natl. Acad. Sci. USA*, 96:13159–13164, 1999.

[13] S. Serowy, S.M. Saparov, Y.N. Antonenko, W. Kozlovsky, V. Hagen, and P. Pohl. Structural proton diffusion along lipid bilayers. *Biophys. J.*, 84:1031–1037, 2003.

[14] A. Springer, V. Hagen, D.A. Cherepanov, Y.N. Antonenko, and P. Pohl. Protons migrate along interfacial water without significant contributions from jumps between ionizable groups on the membrane surface. *Proc. Natl. Acad. Sci. USA*, 108:14461–14466, 2011.

[15] Noam Agmon and Menachem Gutman. Proton fronts on membranes. *Nat. Chem.*, 3:840–842, 2011.

[16] J. Heberle and N.A. Dencher. Surface-bound optical probes monitor proton translocation and surface potential changes during the bacteriorhodopsin photocycle. *Proc. Natl. Acad. Sci. USA*, 89:5996, 1992.

[17] R.E. Lechner, N.A. Dencher, J. Fitter, and Th. Dippel. Two-dimensional proton diffusion on purple membrane. *Solid State Ionics*, 70:296–304, 1994.

[18] M.G. Wolf and G. Groenhof. Explicit proton transfer in classical molecular dynamics simulations. *J. Comp. Chem.*, XX:XX, 2014.

[19] X Kong and C.L. Brooks III. *J. Chem. Phys.*, 105:2414–2423, 1996.

[20] Jennifer L. Knight and Charles L. Brooks, III. lambda-Dynamics Free Energy Simulation Methods. *J. Chem. Phys.*, 30(11):1692–1700, AUG 2009.

[21] Yujie Wu, Hanning Chen, Feng Wang, Francesco Paesani, and Gregory A. Voth. An improved multistate empirical valence bond model for aqueous proton solvation and transport (vol 112B, pg 467, 2008). *J. Phys. Chem. B*, 112(23):7146, 2008.

[22] W.L. Jorgensen, J. Chandrasekhar, J.D. Madura, R.W. Impey, and M.L. Klein. Comparison of simple potential functions for simulating liquid water. *J. Chem. Phys.*, 79:926–935, 1983.

[23] J.S. Hub, M.G. Wolf, C. Caleman, P.J. van Maaren, G. Groenhof, and van der Spoel D. Thermodynamics of hydronium and hydroxide surface solvation. *Chem. Sci.*, XX:XX, 2014.

[24] O. Berger, O. Edholm, and F. Jahnig. Molecular dynamics simulations of a fluid bilayer of dipalmitoylphosphatidylcholine at full hydration, constant pressure, and constant temperature. *Biophys. J.*, 72:2002–2013, 1997.

[25] B. Hess, C. Kutzner, D. van der Spoel, and E. Lindahl. Gromacs 4: Algorithms for highly efficient, load-balanced, and scalable molecular simulation. *J. Chem. Theor. Comp.*, 4:435–447, 2008.

[26] J.P. Ryckaert, G. Ciccotti, and H.J.C. Berendsen. Numerical integration of the cartesian equations of motion of a system with constraints; molecular dynamics of n-alkanes. *J. Comp. Phys.*, 23:327–341, 1977.

[27] S. Miyamoto and P. A. Kollman. SETTLE: An analytical version of the SHAKE and RATTLE algorithms for rigid water molecules. *J. Comp. Chem.*, 18:1463–1472, 1992.

[28] H.J.C. Berendsen, J.P.M Postma, W.F. van Gunsteren, A. DiNola, and J.R. Haak. Molecular dynamics with coupling to an external bath. *J. Chem. Phys.*, 81:3684–3690, 1984.

[29] H.C. Andersen. Molecular dynamics simulations at constant pressure and/or temperature. *J. Chem. Phys.*, 72:2384–2393, 1980.

[30] T. Darden, D. York, and L. Pedersen. Particle mesh Ewald: An N log(N) method for Ewald sums in large systems. *J. Chem. Phys.*, 98:10089–10092, 1993.

[31] MK Petersen, SS Iyengar, TJF Day, and GA Voth. The hydrated proton at the water liquid/vapor interface. *J. Phys. Chem. B*, 108(39):14804–14806, 2004.

[32] D. Van der Spoel, P.J. Van Maaren, P. Larsson, and N. Tîmneanu. Thermodynamics of hydrogen bonding in hydrophilic and hydrophobic media. *J. Phys. Chem. B*, 110:4393–4398, 2006.

[33] F.W. Starr, J.K. Nielsen, and H.E. Stanley. Hydrogen-bond dynamics for the extended simple point-charge model of water. *Phys. Rev. E*, 62:579–587, 2000.

[34] Michael J. Saxton. Anomalous diffusion due to obstacles: A monte carlo study. *Biophys J*, 66:394–401, 1994.

[35] D. Zahn and J. Brickmann. Quantum-classical simulation of proton transport via a phospholipid bilayer. *Phys. Chem. Chem. Phys.*, 3:848–852, 2001.

[36] M. Bonn, H.J. Bakker, A. Ghosh, S. Yamamoto, M. Sovago, and R.K. Campen. Structural inhomogeneity of interfacial water at lipid monolayers revealed by surface-specific vibrational pump-probe spectroscopy. *J. Am. Chem. Soc.*, 132:14971–14978, 2010.

[37] Z. Zhang, L. Piatkowski, H.J. Bakker, and M. Bonn. Interfacial water structure revealed by ultrafast two-dimensional surface vibrational spectroscopy. *J. Chem. Phys.*, 135:021101, 2011.

[38] W. Zhao, D.E. Moilanen, E.E. Fenn, and M.D. Fayer. Water at the surface of aligned phospholipid multibilayer model membranes probes with ultrafast vibrational spectroscopy. *J. Am. Chem. Soc.*, 130:13927–13937, 2008.

[39] Z. Zhang and M.L. Berkowitz. Orientational dynamics of water in phospholipid bilayers with different hydration levels. *J. Phys. Chem. B*, 113:7676–7680, 2009.

[40] S.M. Gruenbaum and J.L. Skinner. Vibrational spectroscopy of water in hydrated lipid multi-bilayers. i. infrared spectra and ultrafast pump-probe observables. *J. Chem. Phys.*, 135:075101, 2011.

[41] E. Flenner, J. Das, M.C. Rheinstädter, and I. Kosztin. Subdiffusion and lateral diffusion coefficient of lipid atoms and molecules in phospholipid bilayers. *Phys. Rev. E*, 79:011907, 2009.

[42] Oleg V. Bychuk and Ben O'Shaughnessy. Anomalous diffusion at liquid surfaces. *Phys Rev Lett*, 74:1795, 1995.

[43] In-Chul Yeh and G. Hummer. Diffusion and electrophoretic mobility of single-stranded rna from molecular dynamics simulations. *Biophys J*, 86:681–689, 2004.

[44] Emile S. Medvedev and Alexei A. Stuchebrukhov. Mechanism of long-range proton translocation along biological membranes. *FEBS Lett.*, 587:345–349, 2013.

[45] Jie Zhang and Patrick R. Unwin. Proton diffusion at phospholipid assemblies. *J. Am. Chem. Soc.*, 124:2379–2383, 2002.

[46] Vitor B.P. Leite, Ailton Cavalli, and Jr. Osvaldo N. Oliveira. Hydrogen-bond control of structure and conductivity of langmuir films. *Phys. Rev. E*, 57:6835–6839, 1998.

[47] Rainer A. Böckman, Agnieszka Hac, Thomas Heimburg, and Helmut Grubmüller. Effect of sodium chloride on a lipid bilayer. *Biophys. J.*, 85:1647–1655, 2003.

[48] Piotr Jurkiewicz, Lukasz Cwiklik, Alžběta Vojtíšková, Pavel Jungwirth, and Martin Hof. Structure, dynamics, and hydration of POPC/POPS bilayers suspended in NaCl, KCl, and CsCl solutions. *Biochim. Biophys. Acta*, 1818:609–616, 2012.

[49] Robert Vácha, Piotr Jurkiewicz, Michal Petrov, Max L. Berkowitz, Rainer A. Böckmann, Justyna Barucha-Kraszewska, Martin Hof, and Pavel Jungwirth. Mechanism of interaction of monovalent ions with phosphatidylcholine lipid membranes. *J. Phys. Chem. B*, 114:9504–9509, 2010.

[50] P. Thomas Vernier, Matthew J. Ziegler, and Rumiana Dimova. Calcium binding and head group dipole angle in phosphatidylserine-phosphatidylcholine bilayers. *Langmuir*, 25:1020–1027, 2009.

[51] Parag Mukhopadhyay, Luca Monticelli, and D. Peter Tieleman. Molecular dynamics simulation of a palmitoyl-oleoyl phosphatidylserine bilayer with na+ counterions and nacl. *Biophys. J.*, 86:1601–1609, 2004.

[52] Andrey A. Gurtovenko and Ilpo Vattulainen. Effect of NaCl and KCl on phosphatidylcholine and phosphatidylethanolamine lipid membranes: Insight from atomic-scale simulations for understanding salt-induced effects in the plasma membrane. *J. Phys. Chem. B*, 112:1953–1962, 2008.

[53] Sun-Joo Lee, Yuhua Song, and Nathan A. Baker. Molecular dynamics simulations of asymmetric nacl and kcl solutions separated by phosphatidylcholine bilayers: Potential drops and structural changes induced by strong na-lipid interactions and finite size effects. *Biophys. J.*, 94:3565?3576, 2008.

[54] Arnau Cordomí, Olle Edholm, and Juan J. Perez. Effect of ions on a dipalmitoyl phosphatidylcholine bilayer. a molecular dynamics simulation study. *J. Phys. Chem. B*, 112:1397–1408, 2008.

[55] Benjamin Klasczyk, Volker Knecht, Reinhard Lipowsky, and Rumiana Dimova. Interactions of alkali metal chlorides with phosphatidylcholine vesicles. *Langmuir*, 26:18951–18958, 2010.

[56] Yanyan Mao, Yun Du, Xiaohui Cang, Jinan Wang, Zhuxi Chen, Huaiyu Yang, , and Hualiang Jiang. Binding competition to the popg lipid bilayer of ca^{2+}, mg^{2+}, na^{+}, and k^{+} in different ion mixtures and biological implication. *J. Phys. Chem. B*, 117:850–858, 2013.

[57] Christopher C. Valley, Jason D. Perlmutter, Anthony R. Braun, and Jonathan N. Sachs. Nacl interactions with phosphatidylcholine bilayers do not alter membrane structure but induce long-range ordering of ions and water. *J Membrane Biol*, 244:35–42, 2011.

[58] Christian Eggeling, Christian Ringemann, Rebecca Medda, Günter Schwarzmann, Konrad Sandhoff, Svetlana Polyakova, Vladimir N. Belov, Birka Hein, Claas von Middendorff, Andreas Schönle, and Stefan W. Hell. Direct observation of the nanoscale dynamics of membrane lipids in a living cell. *Nature*, 457:1159–1163, 2009.

[59] Sangyeon Cho, Jaeduck Jang, Chaeyeon Song, Heeyoung Lee, Prabhakar Ganesan, Tae-Young Yoon, Mahn Won Kim, Myung Chul Choi, Hyotcherl Ihee, Won Do Heo, and YongKeun Park. Simple super-resolution live-cell imaging based on diffusion-assisted frster resonance energy transfer. *Sci. Rep.*, 3:1208, 2013.

[60] S. Gluck. V-ATPases of the plasma membrane. *J. Exp. Biol.*, 172:29–37, 1992.

[61] Clara Franzini-Armstrong and Donald G. Ferguson. Density and disposition of ca^{2+}-ATPase in sarcoplasmic reticulum membrane as determined by shadowing techniques. *Biophys. J.*, 48:607–615, 1985.

[62] K.M. Davies, C. Anselmi, I. Wittig, J.D. Faraldo-Gómez, and W. Kühlbrandt. Structure of the yeast F1Fo-ATP synthase dimer and its role in shaping the mitochondrial cristae. *Proc. Natl. Acad. Sci. U. S. A.*, 109:13602–7, 2012.

[63] Pia Ädelroth and Peter Brzezinski. Surface-mediated proton-transfer reactions in membrane-bound proteins. *Biochim. Biophys. Acta*, 1655:102–115, 2004.

[64] Menachem Gutman and Esther Nachliel. The dynamic aspects of proton transfer processes. *Biochim. Biophys. Acta*, 1015:391–414, 1990.

[65] Lena Böttinger, Susanne E. Horvath, Thomas Kleinschrot, Carola Hunte, Günther Daum, Nikolaus Pfanner, and Thomas Becker. Phosphatidylethanolamine and cardiolipin differentially affect the stability of mitochondrial respiratory chain supercomplexes. *J. Mol. Biol.*, 423:677–686, 2012.

[66] Thomas H. Haines and Norbert A. Dencher. Cardiolipin: a proton trap for oxidative phosphorylation. *FEBS Lett.*, 528:35–39, 2002.

[67] Eugenia Mileykovskaya and William Dowhan. Cardiolipin membrane domains in prokaryotes and eukaryotes. *Biochim. Biophys. Acta*, 1788:2084–2091, 2009.

[68] Simon Ullrich, Sebastian P. Scheeler, Claudia Pacholski, Joachim P. Spatz, and Stefan Kudera. Formation of large 2d arrays of shape-controlled colloidal nanoparticles at variable interparticle distances. *Part. Part. Syst. Charact.*, 30:102–108, 2013.

[69] C. Knight, C.M. Maupin, S. Izvekov, and G.A. Voth. Defining condensed phase reactive force fiels from ab initio dynamics simulations: the case of the hydrated excess proton. *J. Chem. Theory Comput.*, 6:3223–3232, 2010.

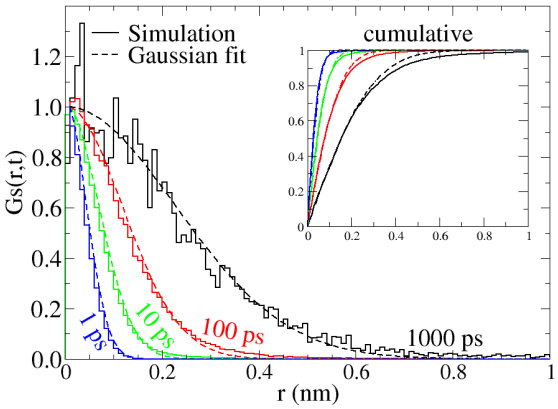

Figure 13: Gs(r,t) of a proton on a membrane surface. The gaussian fits correspond to a normal distributed surface displacement, and the simulation data represent the observed surface displacement.

Supporting information

Gs(r,t)

In addition to the time-dependence of the msd, also the self-part of the van Hove correlation function $G_s(\mathbf{r}, t)$ is an interesting measure to characterize anomalous diffusion. Here, $G_s(\mathbf{r}, t)$ is the probability that a particle has moved within a time span t a distance r. The $G_s(\mathbf{r}, t)$ for a proton on a surface (figure 13) shows that the surface displacement exhibits long-tailed behavior with respect to a normal distribution, indicating anomalous surface diffusion.

Periodic image contribution to autocorrelation function

The autocorrelation function of the hydronium-lipid hydrogen bonds gives the probability that after a certain time interval t the hydronium forms a hydrogen bond with the same lipid. Because we used periodic boundary conditions in our simulation, it is possible that the proton binds to the periodic image of this lipid. As a result, the autocorrelation function would reach a constant value between zero and one, rather than decay to zero.

In our simulations, the probability that the hydronium-lipid hydrogen bond was reformed with a periodic image was negligible. We obtained this probability from the two dimensional diffusion equation, which yields a distribution of 2D displacement,

$$d_{molecule}(r, t) \sim r \exp(-r^2/4Dt), \tag{2}$$

with $4Dt$ the 2D msd at time t and r the displacement. After normalization of the lipid phosphor and the hydronium distribution, the probability to encounter a periodic image

after time t was

$$p(t) = \int_0^{r_{box}} d_{H_3O^+}(r,t) \cdot d_{P_{lipid}}(r_{box} - r, t)dr \tag{3}$$

with r_{box} the smallest box vector (finite size). For instance, at $t = 300$ ps, equation 3 yielded a probability of 10^{-13} for a hydronium in the hb1 ensemble to interact with a periodic image lipid. In the hb2 and hb3 ensemble this probability was even smaller, due to the smaller msd of the hydronium.

Simplified model

In our atomisic simulation of an excess proton in the vicinity of a lipid membrane we find a non-linear relation between the proton mean square surface displacement and time, characterized by an initial subdiffusive regime that was followed by a small superdiffusive regime (figure 4). The diffusion of a proton over a lipid membrane was thus highly anomalous, in contrast to the standard Fickian diffusion observed for a proton moving through bulk solvent.

Multiple phenomena are contributing to the highly anomalous surface diffusion of the proton. First, protons that are bound to a lipid followed the lipid's self-diffusion pattern within the bilayer, which is subdiffusive at short timescales (upto 50 ns)[41]. Second, protons that are trapped in a free-energy well on the surface experienced a local caging effect, which, in combination with a low percolation rate, also leads to a subdiffusive regime[34, 41]. Finally, the strong surface affinity of the proton, with the occasional bulk-mediated long diffusion pathway, typically leads to a superdiffusive regime[42]. The key aspect in these three phenomena is a favorable interaction between the lipids and the proton that results in a reduction of freedom of surface movement. The latter leads to the highly anomalous surface diffusion of the proton.

Remarkably, figure 4 shows that the superdiffusive regime was present only shortly within our simulations and the diffusion quickly became normal (*i.e.* Fickian), rather than extending over a long time-period and approaching the bulk diffusion coefficient [42]. To address this issue, we turned to a simplified model and focused on solutions of the diffusion equation (equation 4), modeled according to the characteristics of our atomistic simulations. Since the free-energy of the proton is not equal throughout the whole system (*i.e.* there is a surface affinity), the flux J in the diffusion equation depends on the chemical potential gradient.

$$\frac{\delta c(r)}{\delta t} = \nabla J \tag{4}$$

$$= \nabla M c(r) \nabla \mu(r) \tag{5}$$

where $\mu(r)$ and $c(r)$ are the chemical potential and the concentration of the excess proton

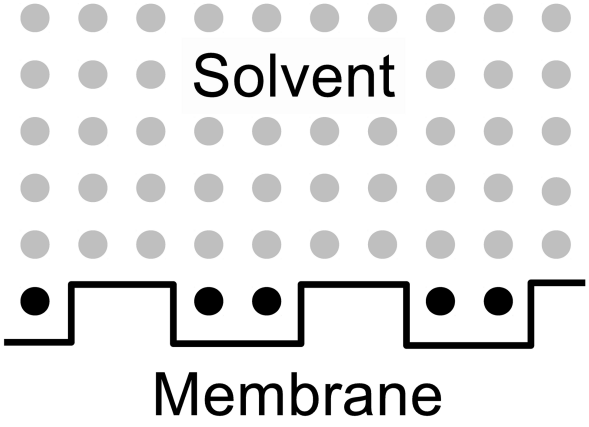

Figure 14: Illustration of the grid used to solve the diffusion equation. Accessible gridpoints are represented by spheres. Black spheres have a lower free-energy than gray spheres. Here, a small part of the grid with a well size of 2 gridpoints is shown.

at location r, respectively, M is a coefficient equivalent to the diffusion coefficient in Fick's diffusion equations, and ∇ represents the vector differential operator del.

We solved the diffusion equation for a 2 dimensional system numerically. Therefore, the evolution of an initial point density on the surface was approximated by performing small timesteps on a grid (figure 14), where we utilized boundary conditions based on the results of our atomistic simulations. The presence of the membrane was represented by an excluded volume for $y < 0$, and the protons surface affinity by a lower free energy associated to the grid points directly adjacent to the excluded volume. To reduce the computational overhead, we used a bulk-to-surface free energy difference of -8 kJ mol^{-1} instead of -13 kJ mol^{-1}, thereby shortening the manifestation of the anomalous diffusion regime. To create the energy wells on the surface that trap the protons, the excluded volume was protruded into the surface adsorption layer periodically. For simplicity, we omitted the proton binding to a lipid molecule and, consequentially, we expected a subdiffusive regime corresponding to the caging effect and a superdiffusion regime due to the occasional bulk-mediated diffusion pathway.

The mean square surface displacement of a proton in this simplified system displayed the same characteristic subdiffusive and superdiffusive regimes that we observed in the atomistic simulations (figure 15). Especially the system with a wellsize of 6 gridpoints compared very well to the results of the atomistic simulations.

In a further comparison between the solution of the diffusion equation and the atomistic simulations we found a discrepancy in the time-dependent diffusion coefficient (figure 16). The diffusion coefficient in the atomistic simulations quickly levels off in the course of our simulations, whereas the diffusion coefficient in the simplified model keaps on increasing

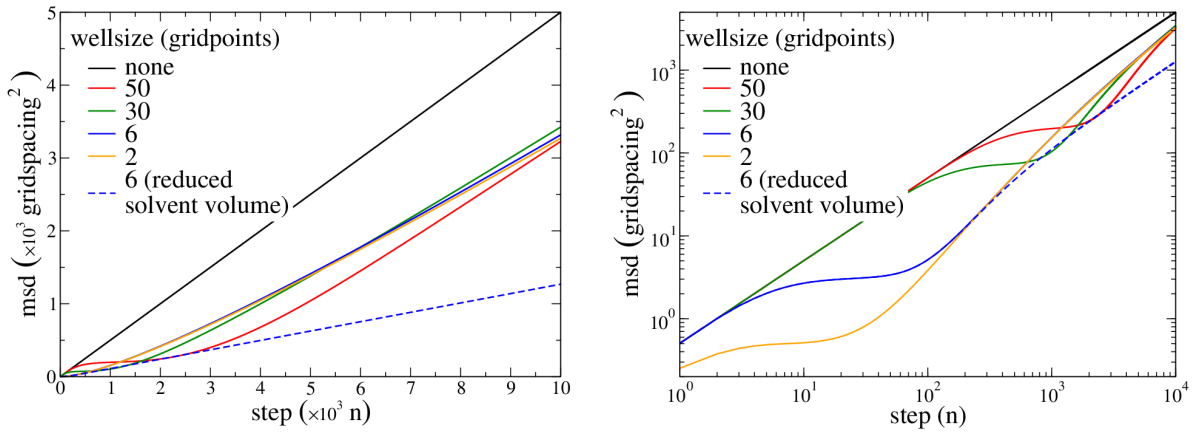

Figure 15: Numerical solutions to the differential equation describing proton diffusion in the vicinity of an adsorbing membrane. The gridsize was `600x600`, the free energy difference between surface and solvent was -8 kJ mol^{-1}, M in the bulk was set to 1 gridpoint^2 step^{-1} and the well-size was varied.

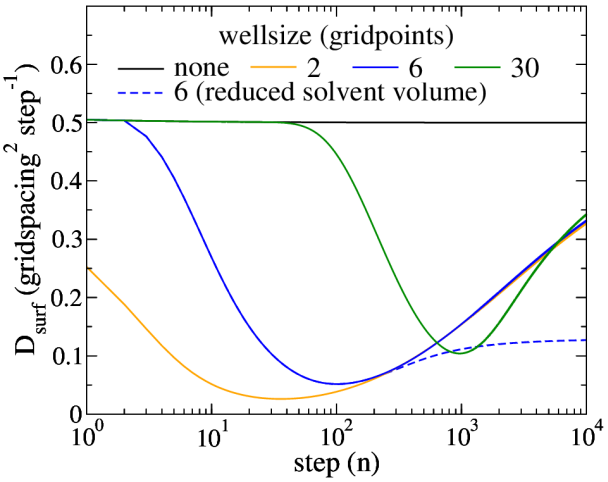

Figure 16: Time dependent diffusion coefficient for surface diffusion on a model membrane. For model parameters see figure 15.

and asymptotically approaches the linear diffusion coefficient of the no-well system. A major difference between the coarse-grained model and the atomistic simulations is the use of periodic boundary conditions in the latter. As a result, a periodic image membrane is present at short distance. After adding a second membrane in the coarse-grained model, the time-dependent diffusion coefficient (dashed line in figure 16) compares much better to that obtained from atomistic simulations. Thus, the periodic image membrane limits the length of the proton bulk excursions, which reduces the contribution of the bulk-mediated diffusion, shortening the superdiffusive regime.

How to experimentally validate bulk-mediated surface diffusion

In this section we propose a possible experiment to distinguish between bulk-mediated and on-surface diffusion of a proton over a membrane. Since the fundamental difference between these two diffusion modes is whether or not a superdiffusive regime appears, we focussed on this aspect in the design of the experiment.

A clear difference between superdiffusion and normal diffusion is the relation between time and msd. On the one hand, a superdiffusion regime leads to a super-linear relation, whereas, on the other hand, normal (Fickian) diffusion leads to a linear relation. By measuring the travel time between a proton source and a proton sensor for various distances, it is possible to experimentally measure the msd as a function of time, and thus to determine the predominant diffusion mode within the measured time- and lengthscale.

Before proposing an experiment we stress that the time- and lengthscale should match that of the onset of the expected superdiffusive regime, because the superdiffusive regime, which approaches a linear asymptot, is indistiguishable from standard diffusion at time- and lengthscale where the msd is close to this asymptot. In our simulations, the superdiffusive regime starts around 1 ns and stretches over an unknown period of time, with a corresponding lengthscale starting around 1 nm^2. Consequently, the experimental time and length scale that we are looking for are a few tens of ns and nm^2. On a lipid bilayer this is almost on the scale of a single lipid, which has a surface area of approximately 0.6 nm^2. Thus the distance between a proton source and a proton sensor can only be a few tens of lipids.

To control the distance between the proton source and the proton sensor on the nm length scale one can think of a rigid linker. Clearly, the resulting linked source and sensor cannot be allowed to interact with other linked pairs, which requires very low concentrations and careful design of the linker to avoid aggregation. This is a considerable challenge, but, if possible, a proper linker would allow the existence of a superdiffusive regime to be tested by varying the length of the linker within the relevant length scale. If the linker distance falls within the superdiffusive regime, a super-linear relation between the square of the linker distance and the time of maximum sensor activity should be observed.

Alternatively, it may be easier to measure the mean distance traveled by the protons from source to sensor in order to determine the dominant diffusion mode. After a single

proton is released on a lipid membrane the average length of the path traveled to reach a sensor will depend on the sensor concentration. Variation of the sensor concentration will change the average distance traveled to a sensor and can thus be used to experimentally determine the relation between time and mean squared displacement. Release and measurement of a single proton is impracticle, but, if one could control the distribution of proton sources into a regular evenspaced array, variation of the sensor concentration should similarly allow to distinguish between a superdiffusive and a normaldiffusive regime.

To determine how the difference in sensor signal will be manifested we modeled such an experimental setup by solving an extended diffusion equation,

$$\begin{aligned}
\frac{\delta c_{H^+}(r)}{\delta t} &= \nabla M c_{H^+}(r) \nabla \mu_{H^+}(r) && (6)\\
&\quad - k_{ass} c_{H^+}(r) c_{sensor}(r) + k_{diss} c_{sensorH}(r) && (7)\\
\frac{\delta c_{sensor}(r)}{\delta t} &= D \left(\frac{\delta^2 c_{sensor}(r)}{\delta x^2} + \frac{\delta^2 c_{sensor}(r)}{\delta y^2} \right) && (8)\\
&\quad - k_{ass} \mu_{H^+}(r) c_{sensor}(r) + k_{diss} c_{sensorH}(r) && (9)\\
\frac{\delta c_{sensorH}(r)}{\delta t} &= D \left(\frac{\delta^2 c_{sensorH}(r)}{\delta x^2} + \frac{\delta^2 c_{sensorH}(r)}{\delta y^2} \right) && (10)\\
&\quad + k_{ass} \mu_{H^+}(r) c_{sensor}(r) - k_{diss} c_{sensorH}(r) && (11)
\end{aligned}$$

assuming the following reaction between the proton and the sensor

$$\mathrm{H_3O^+} + \mathrm{sensor} \rightleftharpoons \mathrm{H_2O} + \mathrm{sensorH^+} \tag{12}$$

with D the surface diffusion coefficient of the (protonated) sensor, which is treated as a constant. Note that the sensor is assumed to be part of the membrane and, hence, diffusion normal to the membrane is not taken into account.

We solved this set of diffusion equations in a similar manner as we did in the case of proton diffusion. We added the (protonated) sensor to the surface layer of our grid model, both inside and outside the wells. The proton association/ dissociation from a sensor located inside or outside a well was related to the surface layer or the bulk, respectively. Within the computational and model limits, we tried to resemble a real system as close as possible, but we note that both the large timestep and the significant simplification make a direct translation of our solution onto a target experiment unfeasible. Instead, our results should rather be interpreted qualitatively.

The diffusion equations were solved on a 80x80 grid using reflective boundary conditions. The gridspacing was 0.1 nm and the timestep 1 ns. The proton and sensor displacement were set to 10^{-2} nm^2 ns^{-1} and 10^{-5} nm^2 ns^{-1}, respectively. Proton adsorption to the surface was set equal to the proton bulk-displacement in one dimension, and proton desorption was derived from $e^{-\Delta G/kT} = \frac{k_{ads}}{k_{des}}$ with $\Delta G = -11.5$ kJ mol^{-1}. The

proton-sensor association constant was set to 1 and the dissociation constant was calculated from $k_{diss} = k_{ass} \cdot K_A$ with K_A the sensor acidity constant set to 6 for the bulk. A bulk pH of 8 was used, and the sensor surface concentration was varied between 10^{-5} and 10^{-1} molecules lipid^{-1}, where one lipid was assumed to occupy eight gridpoints.

The initial steady-state was disrupted by the release of one proton at the origin, corresponding to an approximate release concentration of 1 proton per 100 lipids. The enhanced proton concentration on the surface slowly decays, due to an increased association with the sensor as well as an increased surface desorption. Simultaneously, the concentration of the protonated sensor increases and the concentration of the unprotonated sensor decreases, until a new equilibrium is established. Since the surface desorption is a ceaseless process, this equilibrium cannot be maintained, and the concentration of the proton as well as the protonated sensor starts to fall, whereas the concentration of the unprotonated sensor begins to rise. This turning point in the (protonated) sensor concentration yielded a maximum in the sensors activity.

From the time dependence of the maximum sensor activity as a function of sensor concentration one can distinguish between normal- and super-diffusion. Indeed, when comparing the super-diffusion systems, *i.e.* the well systems, to a normal diffusion system, we observe a different decay profile of the $t_{max\_activity}$ upon increasing concentration (figure 12). Thus systems with a clear superdiffusive regime can be distinguished by the different decay in $t_{max\_activity}$, which is characterized by a second minimum or a shoulder in the plot of the powerlaw exponent α ($\delta \ln t_{max\_activity}/\delta \ln c_{sensor}$).

Regular 2D arrays of small colloidal particles on a substrate [68] may present a suitable base for the array of proton sources; a hydrophobic caged proton (6,7-dimethoxycoumarin-4-yl) [13, 14] can be used as an instantaneous proton source; and Fluorescein [13, 14, 6, 7] or OregonGreen [7] linked to a lipid can be used as a proton sensor.

We remark that an experiment in which neither the proton source nor the proton sensor location is fixed cannot be used to distinguish between superdiffusion and normaldiffusion, because on average there is neither a source nor a sensor gradient on the surface, and, as a result, no net flux of either on the surface. This does not mean that the time to maximum activity cannot be different for distinct diffusion modes, rather the time to maximum sensor activity will not depend on the distance traveled between source and sink, and can thus not be used to find anomalous diffusion.

Finally, we also considered FCS to track the protons surface diffusion. FCS has the advantage that the proton diffusion can be measured in equilibrium [6], but since the diffusion model is used as input to interpret the autocorrelation function of the signal intensity, FCS is only useful if the diffusion mode is known.

Hydroxide parameters

Figure 17 shows a figure of our hydroxide model with the values of the parameters.

Radial distribution function of excess proton in water

To verify whether HYDYN describes the properties of the excess proton in water, we performed HYDYN simulations of the hydrated proton in a small water box and analyzed the trajectory. The intermediate transfer congurations such as the pseudo-Zundel complex, which are observed in a HYDYN simulation, are a clear distinction to non-reactive force field simulations. The consequences for the solvation structure are apparent from the radial distribution functions, shown in Figure 18.

Although the RDF contains the main features of experimental and *ab initio* MD RDFs, there are some differences. The first peak is too narrow and, since HYDYN captures the right coordination number of 3, also too high. The RDF contains a shoulder around 3.2 Å, associated with the waters in the lone-pair region, albeit less pronounced than in *ab initio* MD or MS-EVB3.[69, 21] The peak for the second solvation shell is present, but at too high value. Including polarization (via the SWM4-NDP model) improves the situation somewhat and brings this peak to slightly lower values. The diffusion constant of the excess proton in water at 300 K is $4.4 \cdot 10^{-5}$ cm^2s^{-1},in line with MS-EVB3 results $2.8 \cdot 10^{-5}$ cm^2s^{-1} and experiment $9.3 \cdot 10^{-5}$ cm^2s^{-1}. Therefore, while our model is less accurate than MS-EVB or CPMD with respect to the water structure, it is sufficiently accurate to capture the anomalous diffusion.

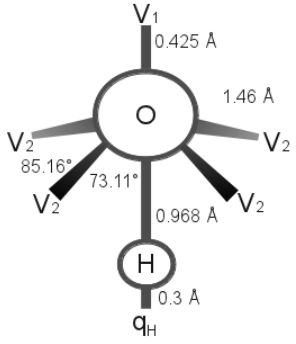

q_O (e)	-1.32
q_H (e)	0.32[1]
ϵ (kcal/mol)	0.0514
σ_O (Å)	-
σ_{V1} (Å)	2.916
σ_{V2} (Å)	2.5
σ_{HH} (Å)	1.1[2] / 1.4[3]

[1]Positioned on q_H site
[2]For combination rule 1
[3]For combination rule 2

Figure 17: Structure and non-bonded parameters of our hydroxide model.

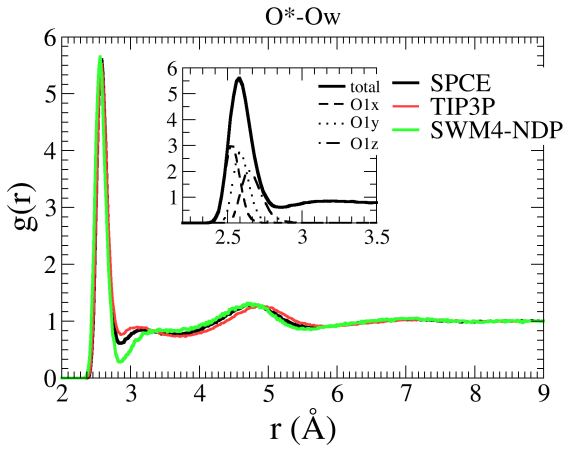

Figure 18: Radial distribution function for the donor-acceptor Oxygen atoms (O*-O) in a HYDYN simulation with different force fields.